IEEE *Access*
Multidisciplinary : Rapid Review : Open Access Journal

Radar Cross Section Analysis of Two Wind Turbines via a Novel Millimeter-Wave Technique and Scale Model Measurements

NIKOLAY LITOV[1], (Student member, IEEE), BEN FALKNER[1], (Student Member, IEEE), HENGYI ZHOU[1], (Member, IEEE), AMIT MEHTA[1], (Senior Member, IEEE), WEZI GONDWE[2], (Member, IMechE), DUSHMANTHA THALAKOTUNA[3], (Senior Member, IEEE), DARIUSH MIRHSEKAR-SYAHKAL[4], (Fellow, IEEE), KARU ESELLE[5], (Fellow, IEEE), HISAMATSU NAKANO[6], (Life Fellow, IEEE),

[1]Swansea University, Bay Campus, Swansea, United Kingdom; SA1 8EN (e-mails: {837921; b.j.falkner; h.zhou; a.mehta}@swansea.ac.uk)
[2]Crossflow Energy, Baglan Bay Innovation Center, Energy Park, Central Avenue, Port Talbot, United Kingdom; SA12 7AX (e-mail: wezig@msn.com)
[3]University of Technology Sydney, Sydney, Australia; NSW 2109 (e-mail: dushmantha.thalakotuna@uts.edu.au)
[4]Essex University, Colchester, United Kingdom; CO4 3SQ (e-mail: dariush@essex.ac.uk)
[5]University of Technology Sydney, Sydney, Australia; NSW 2109 (e-mail: karu.eselle@uts.edu.au)
[6]College of Science and Engineering, Hosei University, Koganei, Tokyo, Japan, 184-8584 (e-mail: hymat@hosei.ac.jp)

Corresponding author: Nikolay Litov (e-mail: 837921@swansea.ac.uk).

ABSTRACT A novel, low cost, highly accurate, millimeter-wave RCS characterization method is developed and presented in this paper. In order to develop and verify the validity of the proposed method, full scale models and scale models of the horizontal-axis wind turbine (HAWT) and Crossflow turbines have been simulated and compared for a case study. The RCS of a scaled Crossflow turbine model was then experimentally verified using the novel method presented at frequencies of 76-81GHz. The proposed method utilizes the AWR1843BOOST evaluation board and DCA1000EVM real-time high-speed data capture card from Texas Instruments. To the best of the authors' knowledge, this is the first RCS analysis of a scaled model performed at the mm-wave frequencies of 76-81GHz. This novel method is quick, simple, and fully automated, while maintaining high accuracy. Additionally, this has been achieved at a low cost using commercially available off the shelf parts. Good agreement was observed between the simulated and experimental results. Comparing the RCS data of the two turbines, it appears that the Crossflow turbine geometry offers a lower RCS and Doppler spectrum contamination as compared with a traditional horizontal axis wind turbine structure. These results are necessary and useful in allaying the increasing concerns regarding wind turbine radar interference, which have appeared as a result of the widespread adoption of wind power generation in recent years.

INDEX TERMS Radar Cross Section, Radar Interference, Wind Turbine Interference, Propagation, Electromagnetic Interference

I. INTRODUCTION

WIND turbines are a strategically important renewable energy resource. Recently, there has been an increase in the adoption of renewable energy sources including wind power [1] [2] as part of a push by many governments towards reducing greenhouse gas emissions and the use of fossil fuels. An increase in installed wind energy generation capacity is necessary in order for us to meet current carbon emission reduction targets [1] [2]. As the number of global wind turbine installations has grown, there have been increasing

reports of wind turbines interfering with neighboring radar installations in various ways [3] [4] [5] [6] [7] [8]. Firstly, wind turbines cause shadowing when they are located within the line of sight of a radar installation, reducing the radar's capability to track targets behind a wind farm. Secondly, the multi-path interference generated can cause the radar to show wind turbine images in places where they are not located. Additionally, due to their blade length, large wind turbines exhibit large blade tip speeds and significant Doppler spectrum contamination as a result [9]. These can often be above the minimum unambiguous velocity detectable by the radar, making them very difficult to filter, and causing the initiation of false tracks in the vicinity of the wind farm.

For all radar wind turbine interference mitigation solutions, it is necessary for the impact on radar installations to be quantified. For this purpose, detailed wind turbine Radar Cross Section (RCS) data is needed. The work in this paper is primarily concerned with monostatic RCS, which can be described as the anisotropic reflectivity of an object in the direction of the incident radiation. As such, the RCS of an object can accurately predict the level of shadowing and clutter that a radar can expect to experience from that object, when it is located in the radar's line of sight. The RCS can be used for the identification and recognition of clutter caused by an object in some cases [12], which makes RCS data useful for the design of filtering algorithms designed to reduce radar interference.

A number of different solutions and mitigation measures have been proposed for the problem of wind turbine radar interference. One of the solutions proposed is the application of radar absorptive coatings and metamaterials to reduce the radar cross section of wind turbines [10] [11]. These solutions however have not been implemented widely at the design and manufacturing stage, and are very costly to apply retroactively to wind turbines that have already been commissioned. Another approach that has been proposed for the reduction of wind turbine-radar interference and that has been used for the RCS reduction of targets generally is that of shaping, i.e. changing the shape of the object in question so that is exhibits a lower RCS. In the case of the wind turbine blades, this is not possible, as aerodynamic performance constraints are the main driver for the blade shape. At the same time, it can be difficult and costly to redesign the tower of the turbine so that it exhibits a lower RCS. Typically, the interference of wind turbines is mitigated via the establishment of exclusion zones around radar installations.

The necessary RCS data can be obtained via simulation, a generally fast, affordable, and accurate solution to the problem [8]. However, it is necessary for simulation results to be verified experimentally. Full scale measurements can be very time consuming and expensive, requiring access to full scale radar installations [5], [13], as well as posing difficulties with controlling the large number of variables. With scale model measurements, it is easier to set up a controlled environment, the experiment takes less time, and is generally cheaper to perform. However, there are still significant costs

associated such as that of building or hiring an anechoic chamber and obtaining a scatterometer system that works at a sufficiently high frequency [14]. Detailed RCS data exists for a variety of widely used wind turbine designs, most notably the horizontal-axis wind turbine (HAWT) geometry with three blades. The Crossflow turbine is a novel wind turbine with various advantages over traditional HAWT designs. The entire Crossflow rotor structure is mounted horizontally on a slew bearing and is driven by motors so that the rotor can be rotated to face the wind to maximize power production, and face out of the wind to reduce the frontal area in extreme wind conditions, thus limiting the loads on the tower and foundation.

In this paper, the first simulation results showing the RCS of the Crossflow turbine are presented, and compared against the RCS results of a commercially available HAWT model with a comparable rated power output. In this comparison, clear advantages for the Crossflow turbine are demonstrated. An experimental validation of results is also presented using the proposed novel millimeter-wave scale model RCS measurement technique, which was realized at a much lower cost than traditional methods [13] [15] [16], while maintaining a high level of accuracy and validity. This was achieved using commercially available off-the-shelf hardware, removing the need for a bespoke scatterometer system. The presented methodology can be used to quickly and accurately characterize scale model structures in a cost effective manner, making it easier to design and rapidly prototype low RCS structures for a variety of applications. Crucially, these measurements have been realized at a high frequency of 76-81GHz. This high frequency allows for both the range and scale model structure to have physically small dimensions. On the other hand, if the system functioned at a lower frequency of 10GHz, the size of such a scale model would have to be in the order of several meters. This poses practical difficulties and is an issue that is resolved by the high frequency method presented in this paper.

In section II, the theory behind the proposed novel RCS characterization method is described. In Section III, simulation results of the radar cross section of two different wind turbine geometries are presented, and the methodology for obtaining these results is also described. In the following Section IV, the proposed RCS characterization method is used to produce an experimental validation of the simulation results. In Section V, a detailed analysis of the results is provided, in addition to recommendations for future work, and a conclusion of the paper.

II. RCS CHARACTERISATION METHOD

The method proposed in this paper builds on the existing literature describing the RCS characterization of scale model structures [17]. Crucially, several novel aspects are introduced which make this method distinct from and preferable to methodologies described in the literature to date. In this section, the mathematical background and theory of scale model radar cross section characterization and an explanation

IEEE *Access*

of how this was leveraged in this scenario is provided first. Secondly, the novel characteristics of the method in both approach and implementation are covered in detail. Finally, any issues and limitations that may arise from this unique approach are examined in detail, and the measures that have been taken to mitigate their impact on the validity and accuracy of the results obtained are provided.

A scale model RCS testing method via comparison is thoroughly described in [17]. Initially, the RCS of the object used as a reference must be defined via the radar equation form seen in Eq. 1.

$$\sigma_{Ref} = (4\pi)^3 R^4 \frac{P_{rRef}}{P_t} \frac{L}{G^2\lambda^2}, \tag{1}$$

where σ_{Ref} is the RCS of the reference object in question, R is the distance between the observing radar system and the object under test, P_{rRef} is the power reflected from the object, P_t is the transmitted power from the observing radar system, G is the gain of the transmitting antenna, L is the overall loss in the system, and λ is the wavelength of operation. For the RCS of the object under test, the RCS equation form shown in Eq. 2 can be used.

$$\sigma_{Obj} = (4\pi)^3 R^4 \frac{P_{rObj}}{P_t} \frac{L}{G^2\lambda^2}, \tag{2}$$

where P_{rObj} is the power received as a reflection from the object under test. The only difference in these two equations is the presence of the P_{rObj} term in Eq. 2 in place of the P_{rRef} term in Eq. 1. This is to denote that the equations concern different scattering objects. As many of the constants in the equations are the same, and antennas which exhibit identical gain are used for transmitting and receiving, the ratio between the RCS of the object under test and the reference object can be expressed as shown in Eq. 3.

$$\frac{\sigma_c}{\sigma_{Ref}} = \frac{(4\pi)^3 R^4 \frac{P_{rObj}}{P_t} \frac{L}{G^2\lambda^2}}{(4\pi)^3 R^4 \frac{P_{rRef}}{P_t} \frac{L}{G^2\lambda^2}} = \frac{P_{rObj}}{P_{rRef}}, \tag{3}$$

Eq. 4, an expression for the RCS of the model under test, can then be derived.

$$\sigma_{Obj} = \sigma_{Ref} \frac{P_{rObj}}{P_{rRef}} = \frac{4\pi a^4}{3\lambda^2} \frac{P_{rObj}}{P_{rRef}} \tag{4}$$

where a is the side length of the trihedral reflector chosen as the reference object. There are a number of conditions which must be observed when performing a scale model RCS measurement [17] [18]:

- Firstly, a minimum distance between the antenna and test subject is specified in Eq. 5 as a function of the largest antenna dimension (D_a) and the largest dimension of the object under test (D_{ob}).
- Secondly, the relationship between the largest dimension of the object under test (D_{ob}) and the wavelength displayed in Eq. 6 must be satisfied, thus ensuring that the object under test is in the optical scattering region.

- Thirdly, the measurements must be conducted in a low reflectivity environment.

$$R \geq 2\frac{(D_a + D_{ob})^2}{\lambda}, \tag{5}$$

$$k\frac{D_{ob}}{2} > 10 \Rightarrow D_{ob} > \frac{10\lambda}{\pi}, \tag{6}$$

In Eq. 6, $k = 2\pi/\lambda$ and is the wave number in free space. P_{rObj} is backcalculated using the raw ADC voltage input values [19] [20]. This is achieved using Eq. 7:

$$P_{rObj} = P_{ADC} - G_{LNA} - G_{Antenna} + FPL, \tag{7}$$

where G_{LNA} is the programmable LNA gain (30dB), $G_{Antenna}$ is the gain of the series fed patch antenna (10.5dBi), and FPL is the free-space path loss (45.9091dB over 0.2m).

The power incident on the scale model, P_{tObj}, can be found using Eq. 8:

$$P_{tObj} = P_{Tx} + G_{Antenna} - FPL, \tag{8}$$

where P_{Tx} is the maximum transmit power of the board (12dBm). The RCS in m^2 can then be calculated using Eq. 9:

$$\sigma = 4\pi R^2 \frac{P_{rObj}}{P_{tObj}}, \tag{9}$$

where R is the distance between the transceiver and the scale model. Finally, the RCS data for the scale model must have a scale factor applied to it [21] in order for us to obtain the full scale values, as shown in Eq. 10.

$$\sigma_{fullScale} dBsm = \sigma_{scaleModel} dBsm + 10log_{10}(n^2), \tag{10}$$

where n is the scale factor applied to produce the scale model.

The presented novel mm-wave RCS characterization method was enabled by the use of the AWR1843BOOST evaluation module from Texas Instruments [22], which offers a 76-81GHz frequency modulated continuous wave radar implementation. The frequency span of the radar module corresponds to wavelengths of 3.9mm to 3.7mm, which satisfy the conditions required for valid measurements outlined previously.

Additionally, the third condition requiring a low reflectivity environment was satisfied by conducting testing in a wide-open area. At the employed frequencies, this constitutes a low reflectivity environment due to the large free space loss values observed in the mm-wave range. At 75 GHz, the free space path loss is approximately 59 dB/m. The RCS measurements were conducted in 0.9° increments. The power scattered by the object in the direction of the transceiver, P_{rObj}, and the power incident on the object, P_t, are measured using the AWR1843BOOST + DCA1000EVM hardware combination.

The technical characteristics of the AWR1843BOOST millimeter-wave radar transceiver and the DCA1000EVM high-speed data capture are favorable for the application described in this work. Firstly, this hardware combination can produce sufficiently high frequencies, operating in the region of 76-81 GHz [22]. Additionally, the hardware has a low receive channel noise figure of 14-15 dB, built-in calibration, 3 Transmit and 4 Receive channels, and a robust software ecosystem allowing for quick and easy development. While the receive channel noise figure may not be considered low compared with more complex systems, this level is acceptable give the other advantages of the system, namely low cost, high measurement speed, and easy integration. The supplied software also allows the user to configure different transmitted chirp profiles for easy prototyping. The hardware has a configurable transmitted bandwidth in the region of 60 MHz to 5 GHz. The transmitted instantaneous bandwidth used in this application was 1.8 GHz. The range resolution achievable by the hardware is as low as 3.25 cm.

The band of 76-81 GHz was chosen due to the scaling requirement which states that the frequency used must be scaled by a factor n, where n is the scale factor of the model; in addition to the commercial availability of the hardware. This band also ensures that the object under test is in the optical scattering region at the corresponding wavelengths, i.e. $l/\lambda \gg 1$, where l is the shortest dimension of the object.

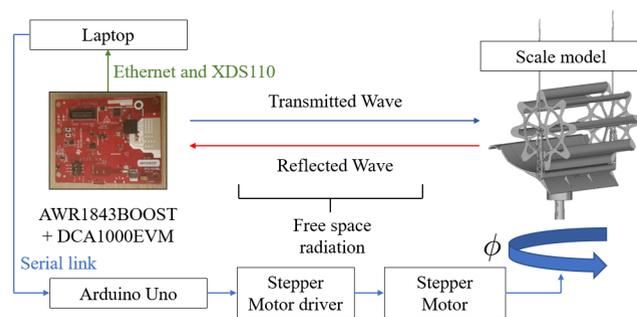The experimental test system setup can be seen in Fig. 1.

FIGURE 1: A diagram describing the experimental setup used for the RCS characterization of the scale model Cross-flow turbine.

The performance of an indoor RCS test range is typically measured using the following parameters [23]:

- **Isolation:** The level of isolation which is achieved with regards to external electromagnetic noise. The test area should be as quiet as possible, so that the only frequencies that contribute to the RCS measurement are those generated by the measurement system and reflected by the target within the RCS test range. In addition to the isolation of external electromagnetic noise, the isolation of other undesired signals must be considered. These include transceiver leakage, coupling between the transmit and receive antennas, reflections from features of the chamber, or chamber-target interactions [16].

TABLE 1: A comparison between the system proposed in this paper and other systems presented in the literature on the basis of their technical characteristics.

Performance indicator	[16]	[15]	[24]	Our work
Type of radar system	Stepped Continuous wave	Pulsed	Pulsed	Continuous wave
Isolation	> 80dB	> 80dB	> 80dB	> 80dB
Quiet zone	0.5m	Not given	Not given	> 1.5m (Constrained only by the attainable open area)
Minimal detectable RCS	Not given	Not given	Not given	$0.2\ m^2$ from mmWave Sensing Estimator
Dynamic range	Not given	Not given	Not given	56dB
Frequency range (Bandwidth)	11 GHz	0.1 GHz	Not given	4 GHz
RCS Accuracy	High	High	High	High
System Design Time	High	High	High	Low
System Portability	Low	Low	Low	High
System Cost	High	High	High	Low
System Complexity	High	High	High	Low

- **Quiet zone:** The quiet zone typically dictates the largest target that can be placed within the indoor RCS test range that satisfies the far field conditions, i.e. still allows for a minimum distance between the transceiver and target necessary for the establishment of far field conditions.
- **Minimum detectable RCS:** The minimum detectable RCS is the smallest RCS that can be measured by the range/system.
- **Dynamic range:** This performance metric provides the difference between the maximum power transmitted by the transmit portion of the transceiver, and the noise floor of the receive portion of the transceiver.
- **Frequency range:** The range of frequencies over which the test system can perform measurements.
- **RCS accuracy:** This performance metric is dependent on the total uncertainty present in the system.

The performance of the new system presented in this paper has been evaluated against other works in the literature using these parameters, and the results are presented in Table. 1. In this table "isolation" refers to the isolation achieved towards electromagnetic signals external to the chamber or range.

Overall, it can be seen that the proposed method and system have several key advantages over methods presented to date in the literature. The most important of these are that

IEEE *Access*

the proposed method is low-cost, low-complexity, and fast. This system can therefore facilitate easy and fast prototyping for a number of different applications, where measurement accuracy is important but not safety critical. These advantages can serve to enable an RCS driven iterative design process.

III. SIMULATION AND ANALYSIS

In order to validate the proposed methodology, two wind turbine geometries were tested and compared - the Crossflow turbine, and a traditional HAWT geometry. The Crossflow turbine CAD model used for the simulation consisted of 150k faces, while the HAWT model was comparatively simpler at 30k faces.
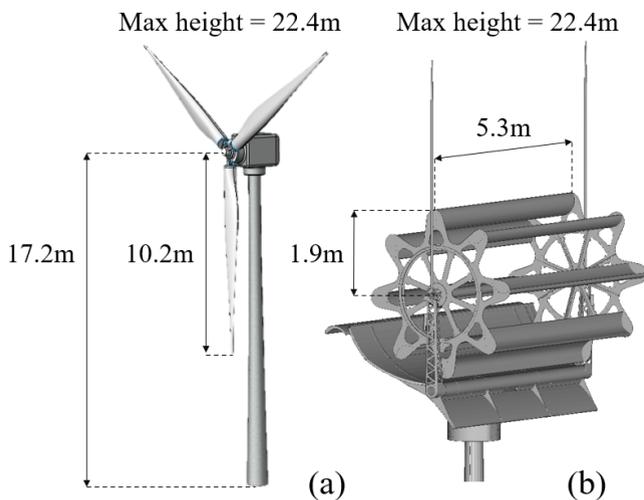

FIGURE 2: An image showing the CAD models of (a) The HAWT, and (b) The Crossflow turbine, together with some of their associated dimensions.

The Crossflow turbine and HAWT models can be seen in Fig. 2. The HAWT model was obtained from a free CAD model repository [25]. The blades of the HAWT are rotated at an angle of 90 degrees such that the trailing edge is in line with the plane of rotation of the blades. The simulation results were obtained using the electromagnetic simulation software Xgtd from REMCOM [26]. This software uses the Physical Optics and Method of Equivalent Edge Currents (PO + MEC) methodology to simulate electrically large scenarios in a computationally efficient manner. Both models were simulated under illumination by linearly polarized (ϕ and θ polarized) plane waves at a frequency of 2.82 GHz, which is the main frequency used by primary surveillance radar (PSR) installations in civilian aviation radar applications.

The simulation scenarios for both turbines, including the plane waves used to illuminate the respective structures can be seen in Fig. 3 (a) and (b). The plane waves used to illuminate the two structures are of different areas, in order to ensure that the entire frontal area of each geometry is illuminated while optimizing the simulation process.
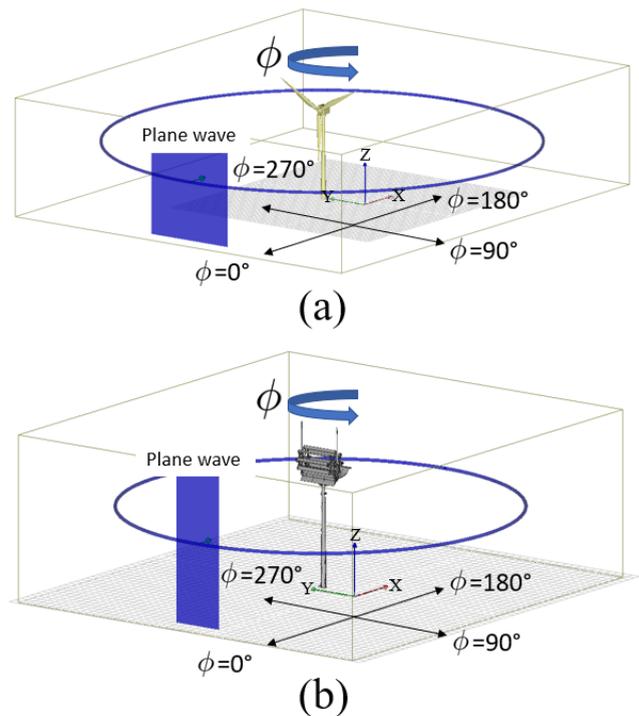

FIGURE 3: An image of the simulation scenario used for the RCS characterization of (a) the HAWT, (b) the Crossflow turbine. Simulation parameters: Frequency = 2.82GHz, Illumination method: Plane wave. Waveform type: Gaussian/chirp. Boundary conditions: Open (non-reflective).
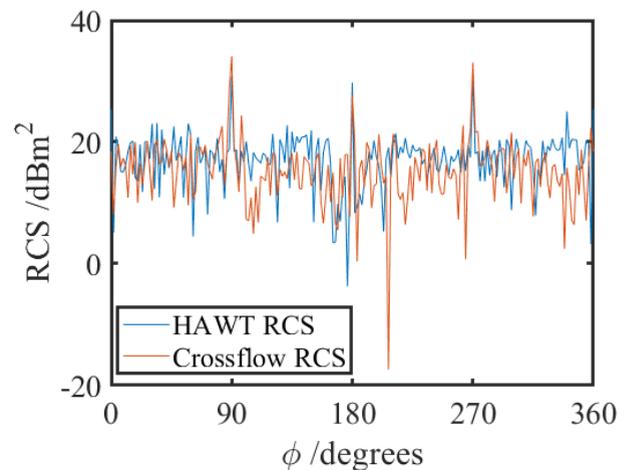

FIGURE 4: A comparison of the HAWT and Crossflow monostatic RCSs, when illuminated by a ϕ polarized plane wave.

This work shows and confirms that the RCS of an object in the optical scattering region is strongly dictated by the geometry of the object. A minima in the RCS of the HAWT at approximately $\phi = 175°$ can be observed in Fig. 4 and 5. This minima can be attributed to the reflectivity characteris-
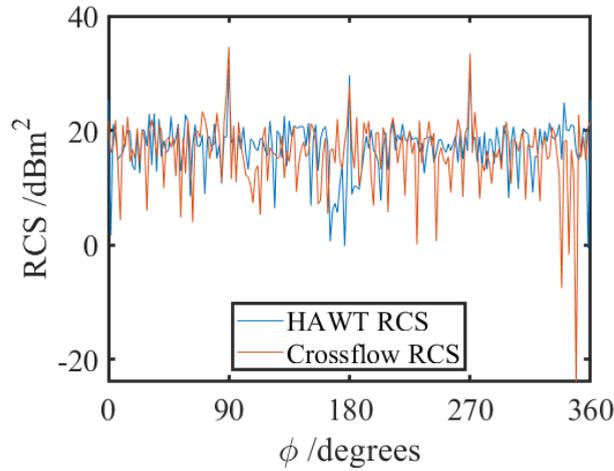
FIGURE 5: A comparison of the HAWT and Crossflow monostatic RCSs, when illuminated by a θ polarized plane wave.

tics and geometry of the individual components of the HAWT and the way in which their reflectivity changes as the aspect angle changes.

Comparison plots with the RCS results of both the Crossflow turbine and HAWT under each polarization can be seen in Fig. 4 and 5. It can be seen that the obtained HAWT RCS results are similar to those presented in the literature [27], [28], [24], [15]. From the presented simulation results, it can be seen that the Crossflow turbine exhibits lower average monostatic RCS values when compared with a traditional HAWT geometry, while the peak RCS for both turbines occurs at the same aspect angles ($\phi = 90°$ and $\phi = 270°$). These results are also supported by the heat maps of the RCS of the Crossflow turbine and HAWT, which can be seen in Fig. 7.

TABLE 2: A table showing a comparison of the physical characteristics of the rotors of the two wind turbine models presented.

Physical characteristic	HAWT	Crossflow turbine
No. of blades	3	6
Blade length	4m	1m
Maximum rotational speed	160rpm	60rpm
Maximum blade tip speed	67.02 m/s	6.28 m/s

TABLE 3: A table showing a comparison of the RCS metrics of the rotors of the two wind turbine models presented under ϕ Polarization.

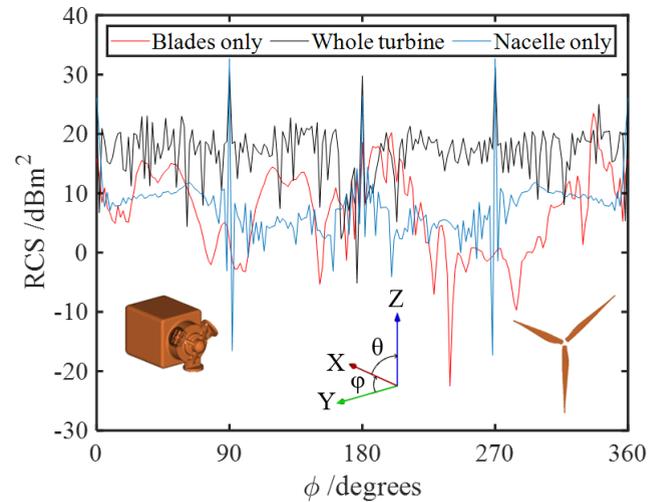| RCS Metric	HAWT	Crossflow turbine	Difference
Peak RCS	31.16dBsm	34.09dBsm	-2.93dBsm
Minimum RCS	-7.25dBsm	-17.41dBsm	10.16dBsm
Average RCS	17.15dBsm	14.54dBsm	2.61dBsm

FIGURE 6: A plot showing the simulated RCS of the horizontal axis wind turbine as well as its various components under ϕ Polarization.

TABLE 4: A table showing a comparison of the RCS metrics of the rotors of the two wind turbine models presented under θ Polarization.

RCS Metric	HAWT	Crossflow turbine	Difference
Peak RCS	31.27dBsm	34.59dBsm	-3.32dBsm
Minimum RCS	-4.56dBsm	-23.89dBsm	19.33dBsm
Average RCS	17.15dBsm	15.47dBsm	1.68dBsm

This is evidenced in the results of the RCS simulations that were conducted of the nacelle and the blades of the HAWT individually. The RCS results of the individual components are overlayed on to the RCS results produced by the turbine simulated as a whole, and this can be seen in Fig. 6. These results shown that the local RCS minima of the blades only and nacelle and blades occur in the same place as they do in the RCS results obtained from the simulation of the entire turbine ($\phi = \sim 175°$). With regards to the maxima of the RCS of the two turbines at $\phi = 90°$, $\phi = 180°$, $\phi = 270°$, these can be attributed to the high reflectivity of the nacelles of the turbines, which is owed to the prominence of flat surfaces in these aspect angles. In carrying out this work and explaining the scattering mechanism that generates the observed RCS plots, some advantages for the Crossflow turbine in terms of monostatic RCS and dynamic Doppler returns have been demonstrated in Fig. 4 and 5 when compared with a HAWT design of comparable dimensions.

To elaborate on the simulation results presented here, two tables are presented comparing key RCS metrics belonging to the two turbines under different polarizations. It can be seen from Tables 3 and 4 that the Crossflow turbine exhibits lower minimum and mean RCS values than the HAWT under both polarizations tested, however it can be seen that the HAWT exhibits a slightly lower peak RCS than the Crossflow
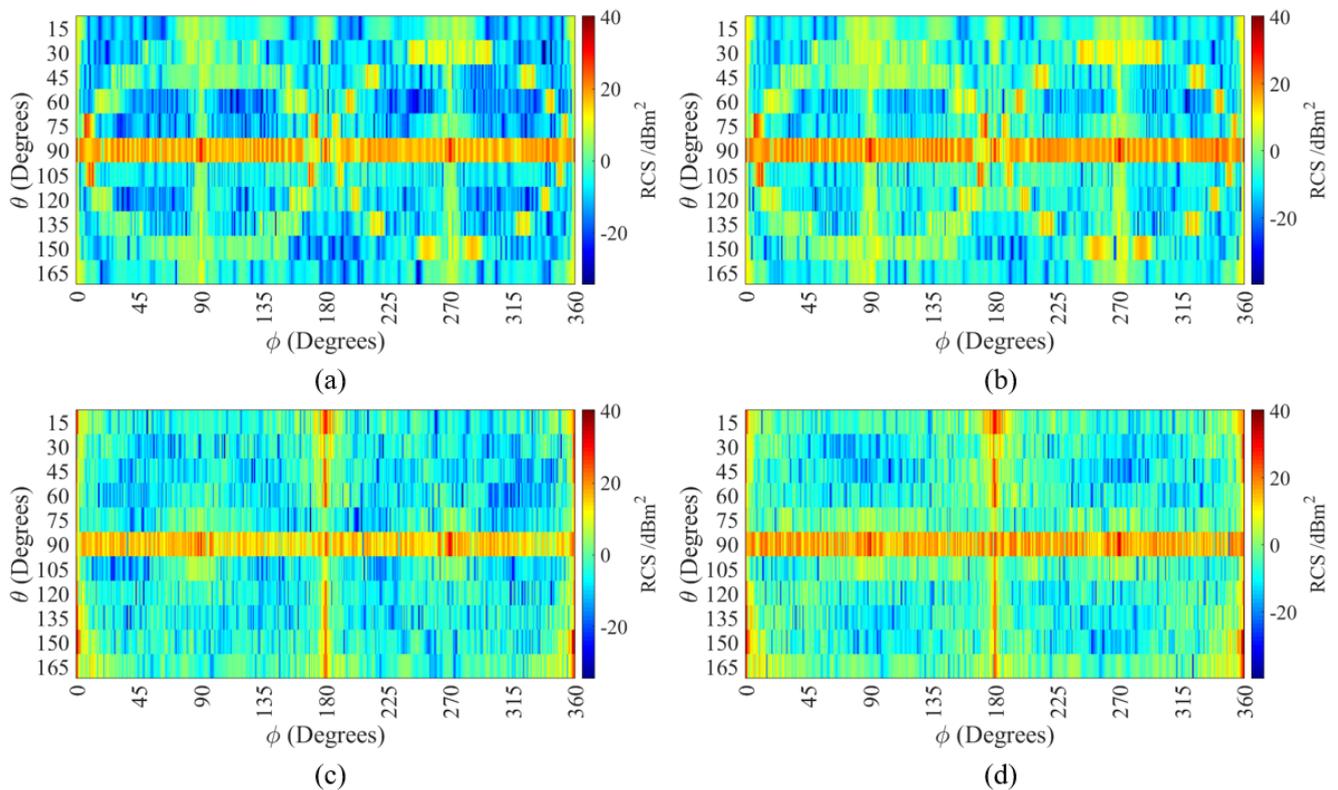
IEEE *Access*

FIGURE 7: A heat map of the RCS of (a) the HAWT under ϕ - polarization, (b) the HAWT under θ - polarization, (c) the Crossflow turbine under ϕ - polarization, (d) the Crossflow turbine under θ - polarization, all for varying ϕ and θ angles.
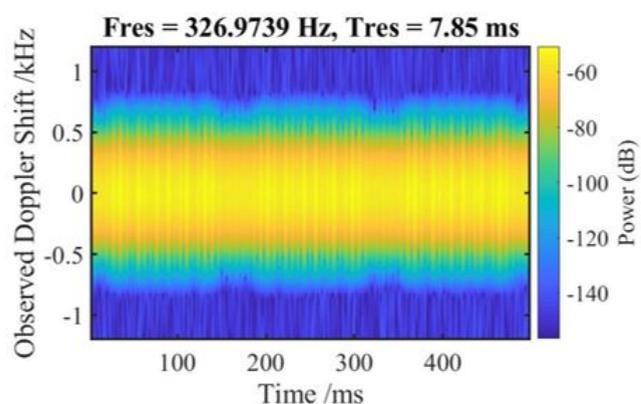
turbine.

As discussed in Section I, Doppler spectrum contamination is one of the major contributors to the interference generated by wind turbines in the vicinity of radar installations. In order to quantify the magnitude of the Doppler returns from the two wind turbine models presented, analytical work was carried out in MATLAB using the Phased Array System Toolbox [29]. The Doppler returns from the two wind turbine models were calculated at the point of maximum rotational velocity, representing a worst case scenario. The reason why maximum rotational velocity is used as the worst-case scenario is that under these conditions, a turbine exhibits its highest blade tip speed, i.e. the maximum linear velocity exhibited by the blade tip in the direction of the radar installation is exhibited under these conditions. The aspect angles at which this is the case are $\phi = 90°$, $\theta = 90°$ for the case of the HAWT, and $\phi = 0°$, $\theta = 90°$ for the case of the Crossflow turbine. Table 2 shows a comparison of the physical characteristics of the two wind turbines. It can be seen from the table that the Crossflow turbine has a lower peak rotational speed and shorter blades, resulting in a significantly lower maximum blade tip speed as compared with the HAWT. This lower peak blade tip speed corresponds to a much lower observed peak Doppler shift. The Time-Doppler plots for the case of the HAWT and for the Crossflow turbine are shown in Fig. 8.

TABLE 5: A table showing the parameters of the two different chirp profiles used during testing.

Chirp Profile Characteristic characteristic	Chirp profile 1	Chirp profile 2
Start frequency	77GHz	77GHz
Frequency slope	29.982 MHz/μs	1.014 MHz/μs
Bandwidth	1798.92MHz	60.84MHz
ADC samples per chirp	256	256
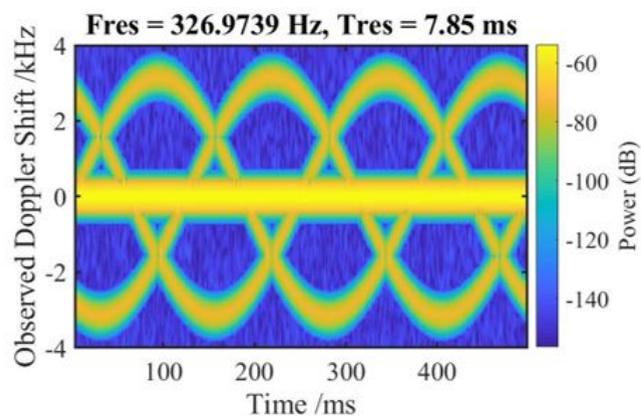
(a)

(b)

FIGURE 8: A time-Doppler plot showing the micro-Doppler returns calculated to be produced by the presented (a) horizontal-axis wind turbine model when it is rotating at its maximum speed of 160rpm, and (b) the Crossflow turbine model when it is rotating at its maximum speed of 60rpm. The aspect angles used were: (a) $\phi = 90°$, $\theta = 90°$, (b) $\phi = 0°$, $\theta = 90°$.

IV. EXPERIMENTAL VALIDATION VIA SCALE MODEL MEASUREMENT

The newly proposed Radar Cross Section (RCS) characterization method (shown in Fig. 9) was used to measure the RCS of a scale model of the Crossflow wind turbine kindly supplied by Crossflow Energy. The novel RCS characterization method presented was used to measure the RCS of a 1:25 scale model of the Crossflow turbine. A comparison between the results obtained using the proposed experimental method and those obtained via simulation can be seen in Fig. 10 for the case of ϕ-polarization and Fig. 11 for the case of θ-polarization. These diagrams show the excellent agreement achieved between the simulated and experimental results. There is good agreement between the average RCS values, as well as between the location and magnitude of the

peak RCS values, observed at $\phi = 90°$ and $\phi = 270°$.

FIGURE 9: A picture of the Crossflow turbine scale model and experimental setup.

These specific areas ($\phi = 90°$ and $\phi = 270°$) have been highlighted because they are considered areas of interest, making them good points at which to perform a direct comparison of the simulated and experimentally obtained results. Generally good agreement is observed in these areas, however there are still some discrepancies that can be observed over certain other aspect angle ranges. The main cause of the discrepancy between the simulated and experimental results is most likely the non-uniform illumination of the target caused by the specific beam pattern of the antennas on the transceiver as opposed to the plane wave illumination used in simulation. To mitigate this limitation of the experimental setup, the scope of the experimental study was limited to the nacelle of the Crossflow turbine only, as the RCS of the tower is consistent across all turbines.
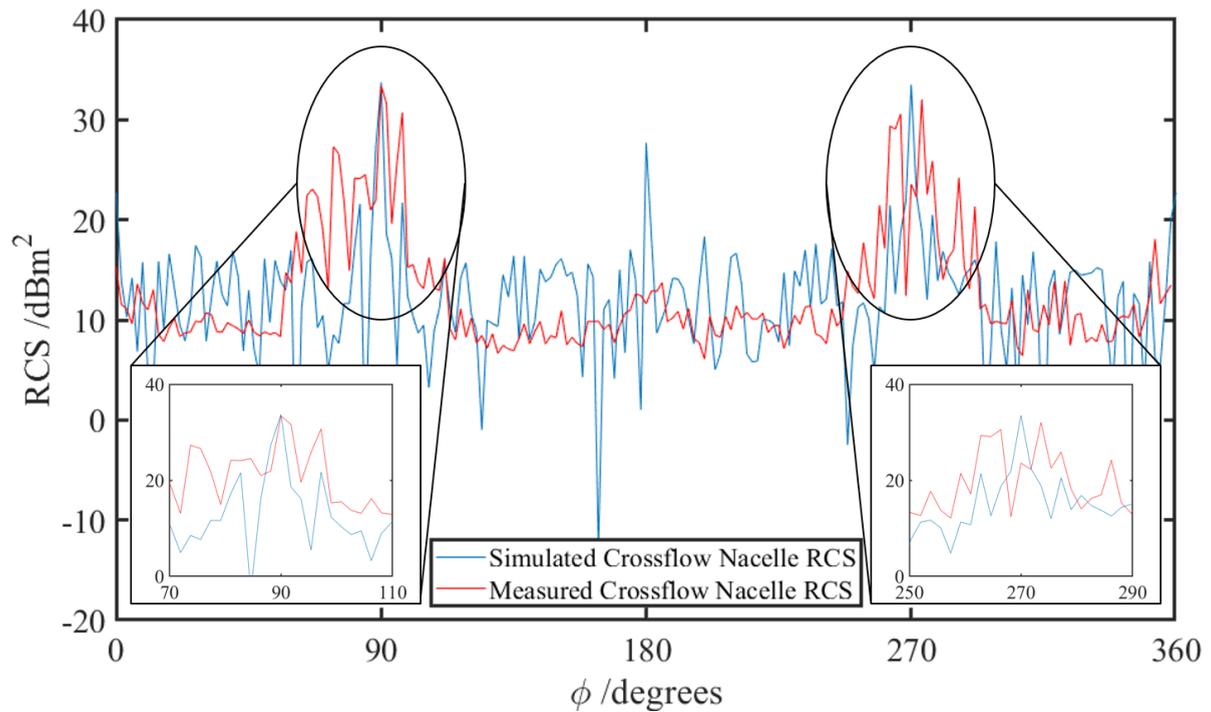
IEEE *Access*

FIGURE 10: A comparison of the experimental and simulated Crossflow turbine nacelle RCS illuminated by a ϕ polarized plane wave, when the averaged values of the 128 chirps at each point are also averaged, creating just a single line for the experimentally measured RCS.

FIGURE 11: A comparison of the experimental and simulated Crossflow turbine nacelle RCS illuminated by a θ polarized plane wave, when the averaged values of the 128 chirps at each point are also averaged, creating just a single line for the experimentally measured RCS.
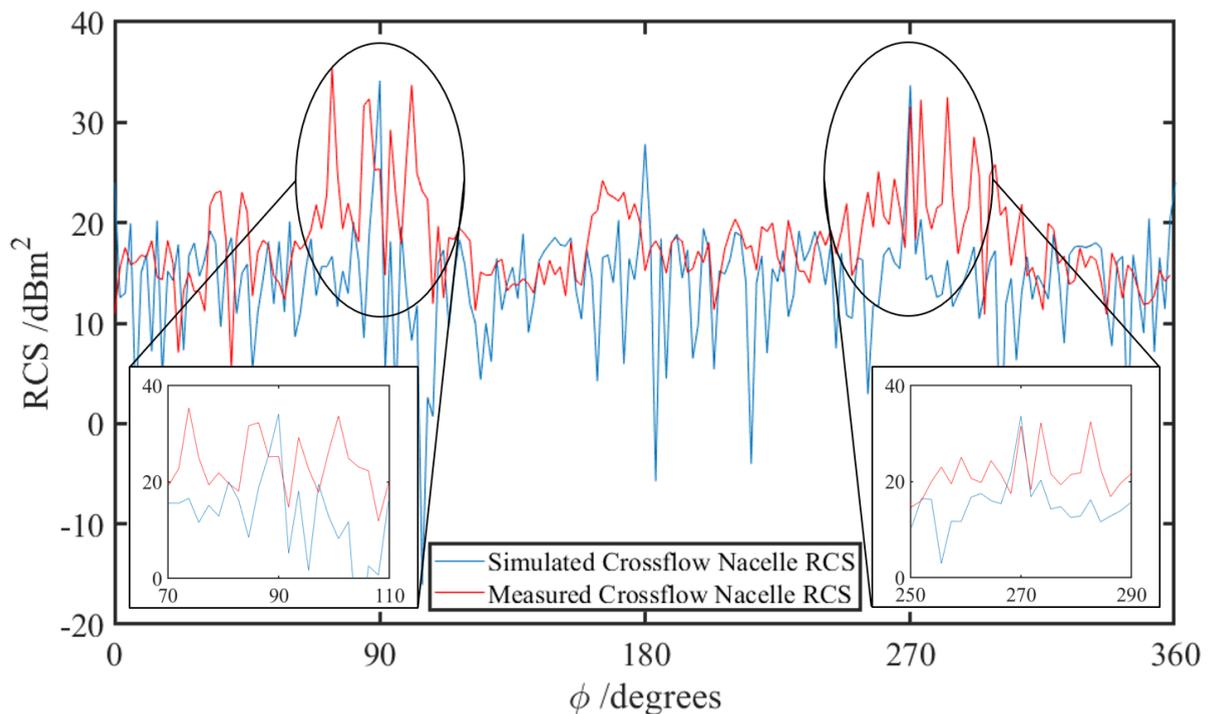
V. CONCLUSION

A novel high-frequency RCS characterization method has been presented. The main advantages of the proposed system are a fast measurement speed, low cost, low complexity, and compact nature. These characteristics make the system ideal for fast and easy prototyping, enabling an RCS driven design process, where measurement accuracy is important but not safety critical. Traditional methods typically require an anechoic chamber, and costly bespoke scatterometer systems. In place of these, a wide open space has been used as a low reflectivity environment, and a cost effective, commercially available radar system have been used in this work. A table comparing this work against others in the literature can be seen in Table 1. Using the proposed method, RCS measurements of a scale model of the Crossflow turbine have been obtained. These results have been compared against the simulation results of the RCS of a traditional HAWT design. Some advantages in terms of lower RCS and lower Doppler spectrum contamination have been demonstrated for the Crossflow turbine, making it more suitable for applications where a low RCS and lower presented radar interference is a concern. Further, good agreement has been observed between the full-scale simulated results and the experimentally obtained scale model results of the Crossflow turbine. This work will also enable the development of novel, low-RCS geometries and designs for a variety of applications such as aviation and ground infrastructure.
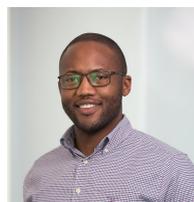
VI. REFERENCES

REFERENCES

[1] International Renewable Energy Agency, "Future of wind", Accessible at: "https://www.irena.org/publications/2019/Oct/Future-of-wind/publications/2019/Oct/Future-of-wind" (accessed Nov. 11, 2020).

[2] R. Best and P. J. Burke, "Adoption of solar and wind energy: The roles of carbon pricing and aggregate policy support," Energy Policy, vol. 118, pp. 404-417, Jul. 2018, doi: 10.1016/j.enpol.2018.03.050.

[3] S. Bachmann, Y. Al-Rashid, P. Bronecke, R. Palmer, B. Isom, and L. Martin, "Suppression of the Windfarm Contribution from the Atmospheric Radar Returns," p. 5.

[4] R. J. Vogt, T. D. Crum, M. J. B. Sandifer, E. J. Ciardi, and R. Guenther, "A Way Forward: Wind Farm Weather Radar Coexistence,"p. 9.

[5] B. M. Isom, R. D. Palmer, G. S. Secrest, R. D. Rhoton, D. Saxion, T. L. Allmon, J. Reed, T. Crum, and R. Vogt, "Detailed Observations of Wind Turbine Clutter with Scanning Weather Radars," Journal of Atmospheric and Oceanic Technology, vol. 26, no. 5, pp. 894-910, May 2009. [Online]. Available:https://journals.ametsoc.org/doi/full/10.1175/2008JTECHA1136.1

[6] B. M. Kent, K. C. Hil, A. Buterbaugh, G. Zelinski, R. Hawley, L. Cravens, Tri-Van, C. Vogel, and T. Coveyou, "Dynamic Radar Cross Section and Radar Doppler Measurements of Commercial General Electric Windmill Power Turbines Part 1: Predicted and Measured Radar Signatures," IEEE Antennas and Propagation Magazine, vol. 50, no. 2, pp. 211-219, Apr. 2008.

[7] Office of the Director of Defense Research and Engineering, "The Effect of Windmill Farms On Military Readiness," Department of Defense, 2006.

[8] N. Litov, H. Zhou, and A. Mehta, "Low Cost Millimetre-Wave Scale Model RCS Characterisation," in 2020 IEEE International Symposium on Antennas and Propagation and North American Radio Science Meeting, Jul. 2020, pp. 1147-1148. doi: 10.1109/IEEECONF35879.2020.9329798.

[9] F. Kong, Y. Zhang, and R. D. Palmer, "Wind Turbine Radar Interference Studies by Polarimetric Measurements of a Scaled Model," IEEE Transactions on Aerospace and Electronic Systems, vol. 49, no. 3, pp. 1589-1600, Jul. 2013, doi: 10.1109/TAES.2013.6558006.

[10] N. Litov, A. Pal, and A. Mehta, "Ring Resonator Metamaterials for Radar Cross Section Reduction," in 2019 IEEE International Symposium on Antennas and Propagation and USNC-URSI Radio Science Meeting, Jul. 2019, pp. 1329-1330, doi: 10.1109/APUSNCURSINRSM.2019.8888700.

[11] H.-K. Jang, W.-H. Choi, C.-G. Kim, J.-B. Kim, and D.-W. Lim, "Manufacture and characterization of stealth wind turbine blade with periodic pattern surface for reducing radar interference," Composites Part B: Engineering, vol. 56, pp. 178-183, Jan. 2014, doi: 10.1016/j.compositesb.2013.08.043.

[12] W. He, C. Ji, Z. Huo, X. Wang and R. Wu, "RCS calculation of wind turbine mast for weather radar," 2016 CIE International Conference on Radar (RADAR), 2016, pp. 1-4, doi: 10.1109/RADAR.2016.8059374.

[13] V. Borkar, A. Ghosh, R. Singh, and N. Chourasia, "Radar Cross-section Measurement Techniques," Defence Science Journal, vol. 60, no. 2, pp. 204-212, Mar. 2010. [Online]. Available:http://publications.drdo.gov.in/ojs/index.php/dsj/article/view/341

[14] Y. Yamada, N. Michishita, and Q. D. Nguyen, "Calculation and measurement methods for RCS of a scale model airplane," in 2014 International Conference on Advanced Technologies for Communications (ATC 2014). Hanoi, Vietnam: IEEE, Oct. 2014, pp. 69-72. [Online]. Available: http://ieeexplore.ieee.org/document/7043358/

[15] F. Kong, Y. Zhang, R. Palmer, and Y. Bai, "Wind Turbine radar signature characterization by laboratory measurements," in 2011 IEEE RadarCon (RADAR), May 2011, pp. 162-166, iSSN: 2375-5318, 1097-5659, 1097-5659.

[16] M. J. Coulombe, T. Horgan, J. Waldman, G. Szatkowski, and W. Nixon, "A 524 GHZ Polarimetric Compact Range for Scale Model RCS Measurements," p. 7.

[17] J. Ochodnicky, Z. Matousek, M. Sostronek, and A. Hykel, "Radar cross section measurement by subscale models," in 2008 International Radar Symposium. Wroclaw, Poland: IEEE, May 2008, pp. 1-4. [Online]. Available: http://ieeexplore.ieee.org/document/4585769/

[18] G. R. Curry, Radar system performance modeling, 2nd ed., ser. Artech House radar library. Boston: Artech House, 2005, oCLC: ocm56672359.

[19] "IWR6843ISK-ODS: Verification of Rx Gain - Sensors forum - Sensors - TI E2E support forums." [Online]. Available: https://e2e.ti.com/support/sensors/f/1023/t/818212?IWR6843ISKODS-Verification-of-Rx-Gain

[20] A. Mani, "Raw ADC data to dBFs."

[21] M. I. Skolnik, "Introduction to radar systems", 2nd ed. New York: McGraw-Hill, 1980.

[22] "AWR1843BOOST Evaluation board | TI.com." https://www.ti.com/tool/AWR1843BOOST (accessed May 30, 2021).

[23] L. Sevgi, Z. Rafiq, and I. Majid, "Radar Cross Section (RCS) Measurements," IEEE Antennas and Propagation Magazine, vol. 55, pp. 278-291, Dec. 2013.

[24] Y. Zhang, A. Huston, R. D. Palmer, R. Albertson, F. Kong, and S. Wang, "Using Scaled Models for Wind Turbine EM Scattering Characterization: Techniques and Experiments," IEEE Transactions on Instrumentation and Measurement, vol. 60, no. 4, pp. 1298-1306, Apr. 2011, conference Name: IEEE Transactions on Instrumentation and Measurement.

[25] "Small-scale HAWT 3D CAD Model Library GrabCAD." [Online]. Available: https://grabcad.com/library/small-scale-hawt-1

[26] REMCOM, "Overview of Remcom's Wind Turbine Research and Capabilities Remcom - Articles and Papers," library Catalog: www.remcom.com. [Online]. Available: https://www.remcom.com/articles-and-papers/overview-ofremcoms-wind-turbine-research-capabilities.html

[27] D. Jenn and C. Ton, "Wind Turbine Radar Cross Section," International Journal of Antennas and Propagation, vol. 2012, pp. 1-14, 2012. [Online]. Available: http://www.hindawi.com/journals/ijap/2012/252689/

[28] L. S. Rashid and A. K. Brown, "RCS and radar propagation near offshore wind farms," in 2007 IEEE Antennas and Propagation Society International Symposium, Jun. 2007, pp. 4605-4608, iSSN: 1947-1491.

[29] "Introduction to Micro-Doppler Effects - MATLAB & Simulink - MathWorks United Kingdom." https://uk.mathworks.com/help/phased/ug/introduction-to-micro-doppler-effects.html (accessed Nov. 17, 2020).

VII. AUTHOR BIOGRAPHIES

NIKOLAY LITOV (Student Member, IEEE) graduated from Swansea Univeristy in 2018 with a First Class Honours BEng Degree. Since then, he has been working towards his EngD Degree from Swansea University. His current research interests include metamaterials, radar cross section measurements, radar interference mitigation, millimeter-wave technology and machine learning for electromagnetics.

BEN FALKNER (Student Member, IEEE) graduated from Swansea University in 2018 with a 2:1 BEng in Electronic & Electrical Engineering. Since then he has been working in the Swansea University Antenna Lab developing wideband antenna solutions for satellite and 5G communication. At the beginning of 2020 he began a PhD on the same topics. In 2019, a paper he presented on a flat panel beam switching linear antenna array for on-the-move GEO satellite communication won best paper award at the 40th ESA Antenna Workshop.

HENGYI ZHOU (Member, IEEE) received MSc. and Ph.D degrees from Swansea University, Swansea, U.K., in 2014 and 2018 respectively. Since 2018, he has been a Research Assistant with the Antenna and Smart City Lab at Swansea University. His current research interests include beam-steerable antennas, phased array antennas, wide-angle-scanning antenna array, GNSS antennas and meta-surface.

AMIT MEHTA (Senior Member, IEEE) received the B.Eng. degree in electronics and telecommunication from the University of Pune, India, and the M.Sc. degree in telecommunications and information networks and the Ph.D. degree in smart reconfigurable antennas from the University of Essex, U.K. He is currently the Professor & Director of the Antenna Research Group, Swansea University, U.K., where his core research interests are wireless communications, and microwave systems and antennas. He is leading large projects teams on 5G, adaptive antennas for GNSS, high throughput satellite communications, IOT, and milli-meter waves. He has successfully supervised over 20 post graduate research theses. He has over 100 technical publications. He holds three patents on the invention of the steerable beam smart antennas and concealed weapons detection systems.

WEZI GONDWE CEng (Member, IMechE) Holds an MSc & BSc in Mechanical engineering from Swansea University. Currently, Wezi designs novel micro renewable energy systems for Cross-flow Energy company. Wezi' s experience is varied, it includes; controls and instrumentation, data acquisition, wind turbine design, data reduction & analysis, and FEA. Before joining his current employer, he worked for an automotive OEM as a process engineer.

DUSHMANTHA N. THALAKOTUNA (M'09-SM'19) obtained his B.Sc. in Electronics and Telecommunication from University of Moratuwa, Sri Lanka in 2008 and PhD in Electronic Engineering from Macquarie University, Australia in 2012.

He is currently a lecturer in School of Electrical and Data Engineering, University of Technology Sydney, Australia. From 2013-2019, he has worked in multiple radio frequency and systems engineering roles designing antennas and MMICs and RF systems for both commercial and defence industries. He is an inventor of three antenna patent applications and authored over 20 refereed journal and conference publications. His current research interests include metasurfaces, reconfigurable antennas, MMICs, Satcom antennas, base station antennas, reconfigurable microwave and millimetre wave circuits and periodic structures.

Dr. Dushmantha was the recipient of several prestigious awards including VIRA Young Scientist in Electronics Award, International Macquarie University Scholarship and CSIRO PhD fellowship. He currently serves as the IEEE NSW section secretary and is a member of Antennas and Propagation Society and Microwave Theory and Techniques Society.

DARIUSH MIRSHEKAR-SYAHKAL (Fellow, IEEE) received the B.Sc. degree (Hons.) in electrical engineering from Tehran University, Tehran, Iran, in 1974, and the M.Sc. degree in microwaves and modern optics and the Ph.D. degree from University College London, University of London, U.K., in 1975 and 1979, respectively. From 1979 to 1984, he was a Research Fellow with University College London, where he was involved in analysis and design of microwave and millimeter-wave planar transmission lines and components as well as on nondestructive evaluation of materials by electromagnetic techniques. Since 1984, he has been on the Staff at the University of Essex, Colchester, U.K., where he is currently a Professor and the Head of the RF & Microwave Research Laboratory, School of Computer Science and Electronic Engineering. He owns several patents and has numerous technical publications, including a book Spectral Domain Method for Microwave Integrated Circuits (New York: Wiley, 1990). He has been a Consultant to more than ten major international companies. His current research interests include adaptive antennas, super-compact RF filters, RF amplifier linearization, characterization, and applications of liquid crystal materials at microwave and mm-wave frequencies, and numerical modeling in electromagnetics and circuits. Dr. Mirshekar-Syahkal is a fellow of the IET and a Chartered Engineer.

KARU ESSELLE (M'92 - SM'96 - F'16) is the Distinguished Professor in Electromagnetic and Antenna Engineering at the University of Technology Sydney and a Visiting Professor of Macquarie University, Sydney. According to 2019 Special Report on Research published by The Australian national newspaper, he is the National Research Field Leader in Australia in both Microelectronics and Electromagnetisms fields.

Karu received BSc degree in electronic and telecommunication engineering with First Class Honours from the University of Moratuwa, Sri Lanka, and MASc and PhD degrees with near-perfect GPA in electrical engineering from the University of Ottawa, Canada. Previously he was Director of WiMed Research Centre and Associate Dean - Higher Degree Research (HDR) of the Division of Information and Communication Sciences and directed the Centre for Collaboration in Electromagnetic and Antenna Engineering at Macquarie University. He has also served as a member of the Dean's Advisory Council and the Division Executive and as the Head of the Department several times. Karu is a Fellow of the Royal Society of New South Wales, IEEE and Engineers Australia.

From 2018 to 2020, Karu chaired the prestigious Distinguished Lecturer Program Committee of the IEEE Antennas and Propagation (AP) Society - the premier global learned society dedicated for antennas and propagation - which has close to 10,000 members worldwide. After two stages in the selection process, Karu was also selected by this Society as one of two candidates in the ballot for 2019 President of the Society. Only three people from Asia or Pacific apparently have received this honour in the 68-year history of this Society. Karu is also one of the three Distinguished Lecturers (DL) selected by the Society in 2016. He is the only Australian to chair the AP DL Program ever, the only Australian AP DL in almost two decades, and second Australian AP DL ever (after UTS Distinguished Visiting Professor Trevor Bird). He has served the IEEE AP Society Administrative Committee in several elected or ex-officio positions 2015-20. Karu is also the Chair of the Board of management of Australian Antenna Measurement Facility, and was the elected Chair of both IEEE New South Wales (NSW), and IEEE NSW AP/MTT Chapter, in 2016 and 2017.

Karu has authored over 600 research publications and his papers have been cited over 11,000 times. In 2020 his publications received over 1,200 citations. His h-index is 52 and i-10 is 191. He is in world's top 100,000 most-cited scientists list by Mendeley Data. Since 2002, his research team has been involved with research grants, contracts and PhD scholarships worth about 20 million dollars, including 15 Australian Research Council grants, without counting the 245 million-dollar SmartSat Corporative Research Centre, which started in 2019. His research has been supported by many national and international organisations including Australian Research Council, Intel, US Air Force, Cisco Systems, Hewlett-Packard, Australian Department of Defence, Australian Department of industry, and German and Indian governments.

Karu's awards include Runner-up to 2020 Australian national Eureka Prize for Outstanding Mentor of Young Researchers, 2019 Motohisa Kanda Award (from IEEE USA) for the most cited paper in IEEE Transactions on EMC in the past five years, 2019 Macquarie University Research Excellence Award for Innovative Technologies, 2019 ARC Discovery International Award, 2017 Excellence in Research Award from the Faculty of Science and Engineering, 2017 Engineering Excellence Award for Best Innovation, 2017 Highly Commended Research Excellence Award from Macquarie University, 2017 Certificate of Recognition from IEEE Region 10, 2016 and 2012 Engineering Excellence Awards for Best Published Paper from IESL NSW Chapter, 2011 Outstanding Branch Counsellor Award from IEEE headquarters (USA), 2009 Vice Chancellor's Award for Excellence in Higher Degree Research Supervision and 2004 Innovation Award for best invention disclosure. His mentees have been awarded many fellowships, awards and prizes for their research achievements. Fifty-five international experts who examined the theses of his PhD graduates ranked them in the top 5% or 10%. Two of his recent students were awarded PhD with the highest honour at Macquarie University - the Vice Chancellor's Commendation.

Karu has provided expert assistance to more than a dozen companies including Intel, Hewlett Packard Laboratory (USA), Cisco Systems (USA), Audacy (USA), Cochlear, Optus, ResMed and Katherine-Werke (Germany).

His team designed the high-gain antenna system for the world's first entirely Ka-band CubeSat made by Audacy, USA and launched to space by SpaceX in December 2018. This is believed to be the first Australian-designed high-gain antenna system launched to space, since CSIRO-designed antennas in Australia's own FedSat launched in 2002.

Karu is in the College of Expert Reviewers of the European Science Foundation (2019-22) and he has been invited to serve as an international expert/research grant assessor by several other research funding bodies as well, including the European Research Council and funding agencies in Norway, Belgium, the Netherlands, Canada, Finland, Hong-Kong, Georgia, South Africa and Chile. He has been invited by Vice-Chancellors of Australian and overseas universities to assess applications for promotion to professorial levels. He has also been invited to assess grant applications submitted to Australia's most prestigious schemes such as Australian Federation Fellowships and Australian Laureate Fellowships. In addition to the large number of invited conference speeches he has given, he has been an invited plenary/extended/keynote speaker of several IEEE and other conferences and workshops including EuCAP 2020 Copenhagen, Denmark; URSI'19 Seville, Spain; and 23rd ICECOM 2019, Dubrovnik, Croatia.

Karu has served as an Associate Editor of IEEE Transactions on Antennas Propagation, IEEE Antennas and Propagation Magazine and IEEE Access. He is a Track Chair of IEEE AP-S 2021 Singapore and AP-S 2020 Montreal, Technical Program Committee Co-Chair of ISAP 2015, APMC 2011 and TENCON 2013 and the Publicity Chair of ICEAA/IEEE APWC 2016, IWAT 2014 and APMC 2000. His research activities are posted in the web at http://web.science.mq.edu.au/ esselle/ and https://www.uts.edu.au/staff/karu.esselle .

HISAMATSU NAKANO (M'75-SM'87-F'92-LF'11) has been with Hosei University since 1973, where he is currently a Professor Emeritus and a Special-appointment Researcher with the Electromagnetic Wave Engineering Research Institute attached to the graduate school. He has held positions as Visiting Associate Professor at Syracuse University (March to September 1981), and Visiting Professor at the University of Manitoba (March to September 1986), University of California, Los Angeles (September 1986 to March 1987), and Swansea University, U.K. (July to September of 2016 to 2019). He has published over 340 articles in peer-reviewed journals and 11 books/book chapters, including Low-profile Natural and Metamaterial Antennas (IEEE Press, Wiley, 2016). His significant contributions are the development of integral equations for line antennas in free space and those for printed antennas, an L-shaped wire/strip antenna feeding method, and the inventions of numerous wideband antennas including body of revolution (BoR) antennas, natural and metamaterial (NM) curl antennas, NM spiral antennas, and NM helical antennas. His other accomplishments include the design of antennas for GPS, personal handy phones, space radios, electronic toll collection systems, RFID, UWB, artificial satellites, and radars. Professor Nakano's parabolic reflector antennas with a center-feed backfire helical radiator and flat antennas with low-profile helical radiators, both for Direct Broadcast Satellite (DBS) programs, have reached a commercial penetration into more than 1,300,000 installations. He received the H. A. Wheeler Award in 1994, the Chen-To Tai Distinguished Educator Award in 2006, and the Distinguished Achievement Award in 2016, all from the IEEE Antennas and Propagation Society. He was also a recipient of The Prize for Science and Technology from Japan's Minister of Education, Culture, Sports, Science and Technology in 2010. Most recently, he was selected as a recipient of the Antenna Award of the European Association on Antennas and Propagation (EurAAP) in 2020. He served as a member of the IEEE APS Administrative Committee from 2000 to 2002 and a Region 10 Representative from 2001 to 2010. He is an Associate Editor of several scientific journals and magazines, including Electromagnetics.

● ● ●